Visual area V4 encodes history dependent attentional effort and single-trial perceptual detection

Authors: Supriya Ghosh* and John H. R. Maunsell

Affiliations: Department of Neurobiology, The University of Chicago, Chicago, Illinois 60637, USA.

*** Correspondence:** sghosh5@uchicago.edu

ABSTRACT

Intense attentional effort improves performance. Neurons in visual area V4 exhibit changes in spike rates that are correlated with effort, selective attention and absolute reward expectation. How neuronal spikes in V4 encode attentional states and perceptual performance with reference to other task relevant motivational and decision signals is poorly understood. We recorded neuronal spikes from monkey visual area V4, and isolated attentional effort from reward expectancy and motor decisions in a visual orientation detection task using a statistical approach based on generalized linear models. We found that V4 spike responses exhibit hysteresis with reward changes. Single trial spiking activity encodes a combination of temporally overlapping sensory and cognitive signals. Neuronal spikes integrate contextual history of attentional effort on a longer time scale, and task related perceptual detection in a shorter timescale within a single trial. Notably, immediate reward expectation and behavioral choice probability are poor predictors of V4 spikes throughout the trial. Further, detection of task relevant perceptual signal is decoded from single trial population spikes with high accuracy. These results provide a detailed representation of perceptual and cognitive signals in V4 that are crucial for performance.

KEYWORDS

Attentional effort; reward; visual cortex; single-unit recording

INTRODUCTION

The modulation of neuronal responses by spatial or featural attention has been examined extensively in area V4 in monkey visual cortex. When a monkey's attention is directed towards the receptive field (RF) location of a V4 neuron, improvement in perceptual performance in that region is accompanied by several changes in neuronal activity. Typically, spike rates are greater (Luo and Maunsell, 2015; Moran and Desimone, 1985); individual response variance is reduced; and pairwise spike correlations (noise correlation) decrease (Cohen and Maunsell, 2009; Reynolds and Heeger, 2009). Similarly, responses of V4 neurons can be augmented when an animal increases it attentional effort (the intensive aspect of attention) when faced with a more challenging task (Boudreau et al., 2006; Spitzer et al., 1988).

However, interpreting neuronal correlates of attention is challenging because it is so closely intertwined with many cognitive and experimental covariates, such as stimulus features, action planning and reward parameters. Expectation of a potential reward is one of the primary external motivators for an animal engaged in a laboratory task. Information about rewards has been reported to exist in many brain structures, including visual areas that are affected by changes in attentional states. Spike rates of neurons in visual cortical area V4 and the lateral intraparietal cortex (LIP) can follow absolute reward size associated with a visual target inside their RFs in a manner independent of attentional performance (Baruni et al., 2015; Rorie et al., 2010). Neuronal encoding of expected reward or choice is well studied in the striatum (Schultz et al., 1992; Tremblay et al., 1998) and prefrontal cortex (Donahue and Lee, 2015; Padoa-Schioppa and Assad, 2006; Roesch and Olson, 2004), and is characterized by neuronal activity correlated with the absolute reward contingency associated with a stimulus while being independent of the relative reward value. Because attention and reward are both defined by their action on goal-directed behavior, their high

47 covariance in relation to performance makes it difficult to isolate the true nature of the
48 representation of attention states within the visual cortex.

49 The contribution of visual cortical neurons in encoding attention is typically examined by
50 instructing the animal to direct attention in one way within a block of trials using different, fixed
51 reward conditions, which vary between blocks. This allows animals to attain a stable cognitive
52 state of reward expectation as well as attention. In studies aimed at understanding neuronal
53 encoding of relative versus absolute reward sizes, different reward conditions are often interleaved
54 across trials and signaled by a cue at the start of each trial. Such task designs effectively rule out
55 contributions due to slowly varying or history-dependent attentional effort that changes over
56 several trials. In this framework, the cognitive state of attentional effort may not settle to a stable
57 level, limiting the animal's ability to take advantage of perceptual benefits of intense attentional
58 effort (or economic utilization of costly cognitive resources) in the case of large over small rewards
59 (Baruni et al., 2015; Rorie et al., 2010) (but see (Cicmil et al., 2015)). Thus, in order to define
60 attention quantitatively, it is crucial to understand how neurons represent attentional effort and its
61 transitions in relation to global physiological cognitive state. To do so, one must first define and
62 experimentally control the cognitive effort that manifests across neuronal, physiological and
63 perceptual performance levels. It is additionally crucial to identify how both steady-state and
64 transitions in attentional effort (e.g. high-to-low or low-to-high) correlate with neuronal,
65 physiological and behavioral responses. Finally, it is important to isolate the relative contributions
66 of different task-relevant cognitive and experimental covariates to visual cortical spikes within a
67 single trial as the trial progresses.

68 We manipulated the level of monkeys' attentional effort using a novel task in which their
69 overall attentional effort was switched between high and low levels with no change in attentional
70 selectivity for stimuli at one location over another. We found that attentional effort modulates V4

neurons independently of spatial or featural attention. Additionally, by varying reward size on each trial around an average, we could produce a single trial estimates of reward expectation as well as both the transient and stable (slow-varying) attentional effort. Using a generalized linear model (GLM) on single trial spike-counts of individual V4 neurons, we quantitatively described contributions of temporally overlapping neuronal response components associated with attentional effort, reward expectation and perceptual detectability. This framework revealed both steady state and time varying signals encoded in V4, enabling the assessment of a broader spectrum of cognitive functions to which visual cortical areas can contribute dynamically.

RESULTS

Reward size modulates attentional effort

We trained two rhesus monkeys to distribute their visual spatial attention between the left and right hemifields while doing an orientation detection task (**Figure 1A**). The animal held its gaze on a central fixation spot throughout each trial. Two Gabor sample stimuli appeared briefly (200 ms) after a randomly varying period of fixation and, after a subsequent delay (200-300 ms), a single Gabor test stimulus appeared at one of the two sample locations (selected pseudo-randomly). If the orientation of the test stimulus differed from the sample that had appeared in that location (a target) the monkey had to rapidly make a saccade to the stimulus to earn a juice reward. On a random half of the trials, the orientation of test stimulus was unchanged (a non-target) and the monkey was required to maintain fixation. In that case, a second test stimulus that always had a different orientation was presented after a short delay and monkeys needed to saccade to this stimulus to earn a reward. Reward values for correct responses were always the same on both sides and fixed, either small or large, within alternating blocks of 120 trials. Stimulus parameters remained unchanged throughout all trial blocks within a session except the reward size. The transitions between blocks were unsignaled and sequential (small to large or large to small, **Figure**

95 **1B**). The monkey therefore had to estimate reward expectancy based on previous trials to adjust

96 its behavioral strategy in allocating effort between blocks.

97 Varying rewards in different blocks of trials allowed us to behaviorally control the amount

98 of attention the animal directed to each stimulus location. Animals were encouraged to maintain a

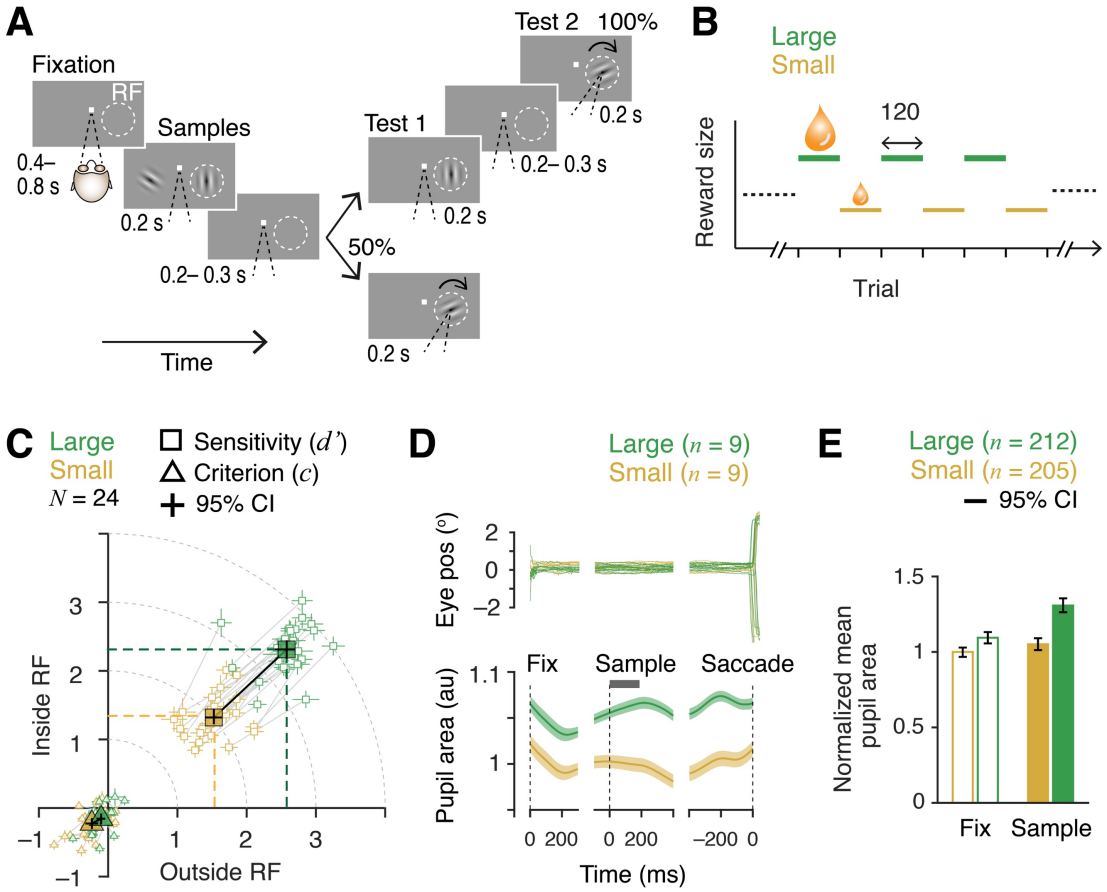

Figure 1. Manipulation of attentional effort using differential reward outcomes. (**A**) Visual spatial attention task. Monkeys were required to fixate, attend to sample stimuli (Gabors) presented in both hemifields (inside and outside of recorded neurons' receptive field (RF)) and report an orientation change that occurred in one of the two test intervals by making a saccade to the stimulus location. (**B**) Unsignaled change in reward size between large and small values over blocks of 120 trials. (**C**) Attention operating characteristic (AOC) curve, indicating behavioral sensitivity (*d'*, circles) and criterion (*c*, triangles) on individual sessions and their average (solid markers) for test stimuli inside and outside RF during two reward conditions, large and small (24. Total sessions: 9 monkey P; 15 monkey S). Dotted colored lines indicate average *d'* in each hemifield. Lines connect two reward conditions within a session. Error bars, 95% confidence intervals. (**D**) Eye positions (*top*) and pupil areas (*bottom*) aligned to trial events in an example session. Each of 9 blocks, 120 trials/ block. Error bars, 95% confidence intervals. (**E**) Block averaged pupil area during pre-stimulus fixation and sample stimulus periods. Pupil area was normalized to mean of pre-stimulus fixation during small reward trial blocks. Error bars, 95% confidence intervals.

behavioral target/non-target bias (criterion, *c*) close to zero by providing rewards of different sizes for hits and correct rejections (**Figure S1**). Because the reward sizes for targets were always the same in both hemifields, animals typically allocated equal attention to both sides within either the high and low reward condition. Figure 1c plots behavioral sensitivity (*d'*) and response criterion (*c*) for behavioral performance on the first test stimuli on the left and right side for the large and small reward conditions. Solid lines join average sensitivities from alternating high- and low-reward blocks from a single day. Dashed arcs around the origin mark isopleths of constant total effort across the two stimulus locations. Movements perpendicular to these lines correspond to changes in attentional effort; movements along these lines correspond to changes in attentional selectivity. Sensitivities on both locations are well balanced (no net attentional selectivity) during most individual sessions. Larger rewards strongly motivated the animals to increase their attentional effort compared to small reward trial blocks. A four-fold increase in reward size (median small reward 131 µl, quartiles 108 and 150 µl; median large reward 522 µl, quartiles 469 and 570 µl) increased overall behavioral *d'* (Methods) by 71% (mean small 2.03, SEM 0.07; mean large 3.48, SEM 0.08, $p < 10^{-17}$, paired t-test; **Figure 1C**, **Table S1**). Behavioral response criterion remained near zero regardless of reward size (**Figure 1C**, **Table S1**).

Non-luminance mediated task-evoked modulation of pupil size is commonly considered a proxy for mental effort across species (Beatty, 1982; Piquado et al., 2010) (for review (Laeng et al., 2012)). Throughout the task, animals maintained a stable fixation (example session in **Figure 1D**, *top*), during which pupil area remain elevated for large reward trials relative to small reward trials (example session in **Figure 1D**, *bottom*). Large reward increased pupil area during fixation by 9% (all values normalized to fixation on small reward trials, mean large 1.09, SEM 0.02) and during sample stimuli by 24% (mean small 1.05, SEM 0.02, mean large 1.31, SEM 0.02) (repeated measures ANOVA, $F_{(1, 415)} = 45.5$, $p < 10^{-10}$; **Figure 1E**). While the within block trial-averaged

behavioral *d'* was strongly positively correlated with both reward size and pupil area during sample stimuli, pupil area failed to exhibit any correlation with reward size (partial correlation, reward - *d'*, $\rho = 0.68$, $p < 10^{-55}$; pupil area - *d'*, $\rho = 0.23$, $p = 10^{-5}$; reward - pupil area, $\rho = 0.08$; $p = 0.09$; $N = 417$ blocks of trials).

Responses of V4 neurons increase with increasing attentional effort

Some previous studies have shown that attention-related modulation of the responses of V4 neurons increases when tasks demand more cognitive effort (Boudreau et al., 2006; Spitzer et al., 1988). However, in those studies increases in task difficulty always covaried with increases in behavioral selectivity for one visual field location over another. A more recent study similarly showed that the neurons in V4 respond more strongly when monkeys shift their attention to increase their behavioral *d'* at the recorded neurons' receptive field location relative to another location in the opposite hemifield (Luo and Maunsell, 2015), a manipulation that also covaried selectivity and sensitivity. Our task design allowed us to change attentional effort with no appreciable change in the selectivity for one spatial location over the other (**Figure 1C).**

We recorded 970 single units and small multi-unit clusters during 24 recording sessions from the two monkeys (monkey P, 9 sessions, 407 units; monkey S, 15 sessions, 563 units) using 96 channel multielectrode arrays chronically implanted in V4 in the superficial prelunate gyrus of one hemisphere. Trial averaged population spike rates during the sample stimuli period for correctly completed trials (hits and correct rejections) increased in large reward trial-blocks when the monkeys' attentional effort was higher (**Figure 2A-C**). Average responses were low because the stimulus was patently suboptimal for most of the simultaneously recorded neurons. The peak-normalized population spike rates in one monkey (animal S) show greater sustained activity than the other (animals P, **Figure 2B, C**). This difference arose from differences in average absolute peak firing rate (monkey P mean 28.7 SEM 1.1 spikes/s, monkey S mean 24.6 SEM 0.9 spikes/s,

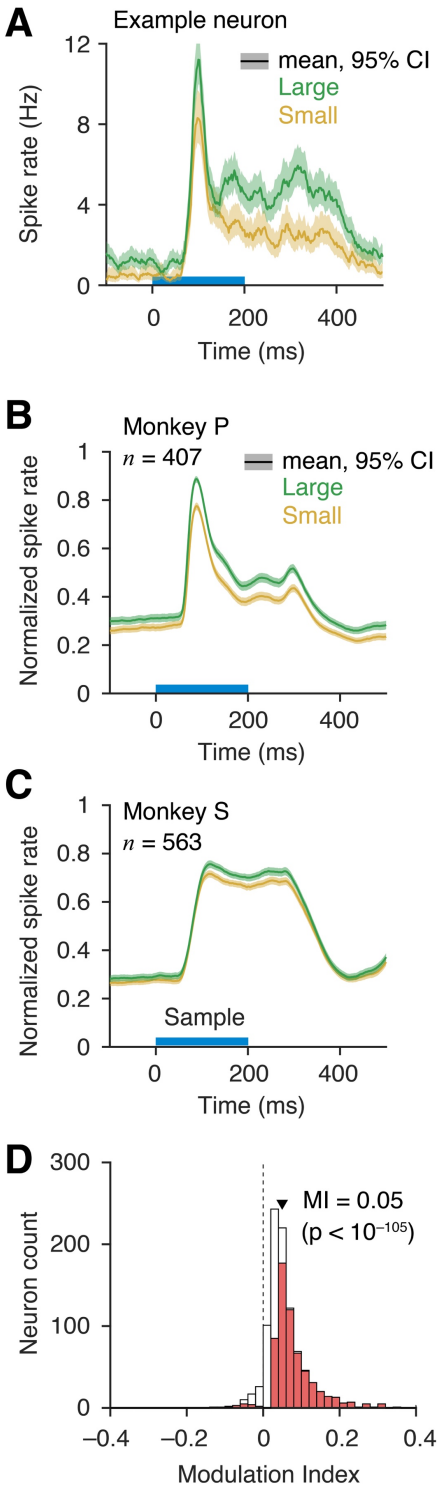

Figure 2. Higher attentional effort increased spiking of neurons in area V4. (**A**) Peri-stimulus time histograms (PSTH) of spike rates of correct trials in large and small reward blocks for an example neuron in V4. Single trial spike counts were binned at 2 ms, smoothed with $\sigma = 15$ ms half-Gaussian and then aligned at the onset of sample stimulus. Horizontal bar, sample stimulus presentation. (**B-C**) Population PSTHs for monkey P (B) and monkey S (C). For population average, spike rates of each neuron were normalized to its peak response within 60 - 260 ms from sample stimulus onset (monkey P, $n = 407$; monkey-S, $n = 563$). Error bars, 95% confidence intervals (bootstrap, $n = 10^4$). (**D**) Distribution of neuronal modulation indices (MI) of all units from both monkey P and S ($n = 970$). Red bars, neurons with MI values significantly different from 0 ($n = 603/970$, $p < 0.05$). White bars, non-significant MI. Solid triangle, population MI averaged across all units ($n = 970$, $p < 10^{-105}$, t-test).

$p < 0.01$, ranksum test) and average absolute sustained rates (monkey P mean 16.2 SEM 0.7 spikes/s, monkey S mean 18.5 SEM 0.6 spikes/s, $p < 0.01$, ranksum test). Principal component

150 (PC) analysis of spike peri-stimulus histograms of all neurons revealed that monkey P has higher
151 principal component scores associated with third PC, which captured transient peak response
152 (**Figure S2**). To quantify neuronal modulation by attentional effort, we computed a modulation
153 index (MI) as the difference of firing rates (60-260 ms from sample onset) between high effort
154 (large reward) and low effort (small reward) conditions divided by their sum. The mean MI was
155 significantly greater than zero, indicating higher firing rates during high effort condition (mean =
156 0.05, $p < 10^{-105}$, $n = 970$, t-test; **Figure 2D** or ~11.6% increase in firing rate). The attentional effort
157 effect was also significant for individual monkeys (monkey P, mean = 0.08, $p < 10^{-70}$; monkey S,
158 mean = 0.03, $p < 10^{-52}$; **Figure S3**). In addition, of 970 units recorded in V4 in the two monkeys,
159 significant effort modulations ($p < 0.05$) were observed in 603 (62%) units. Thus, an isolated
160 change in attentional effort affects responses in V4 in absence of behavioral selectivity or response
161 criterion changes.

162 **Trial-by-trial physiological and behavioral dynamics in response to reward modulation**

163 Many experimental covariates might closely follow the timing of changes in reward size. We
164 therefore examined the dynamics of neuronal, physiological and behavioral responses associated
165 with reward changes. Trial-by-trial values of behavioral *d'*, sample-stimuli-evoked pupil area and
166 spike counts were aligned to the first correct trial after block transitions, and then averaged across
167 blocks (**Figure 3**). The first reward in a block unambiguously signaled a block transition, which
168 was otherwise unannounced. Block-averaged single trial reward values received by the animals
169 approximated step functions (single exponential fit: $\tau = 0.2$ and 0.5 trials respectively for
170 transitions from small-to-large ($n = 212$ blocks) and from large-to-small ($n = 205$ blocks), **Figure**
171 **3A**). Behavioral *d'* closely tracked reward changes for the transition from large-to-small ($\tau = 1$).

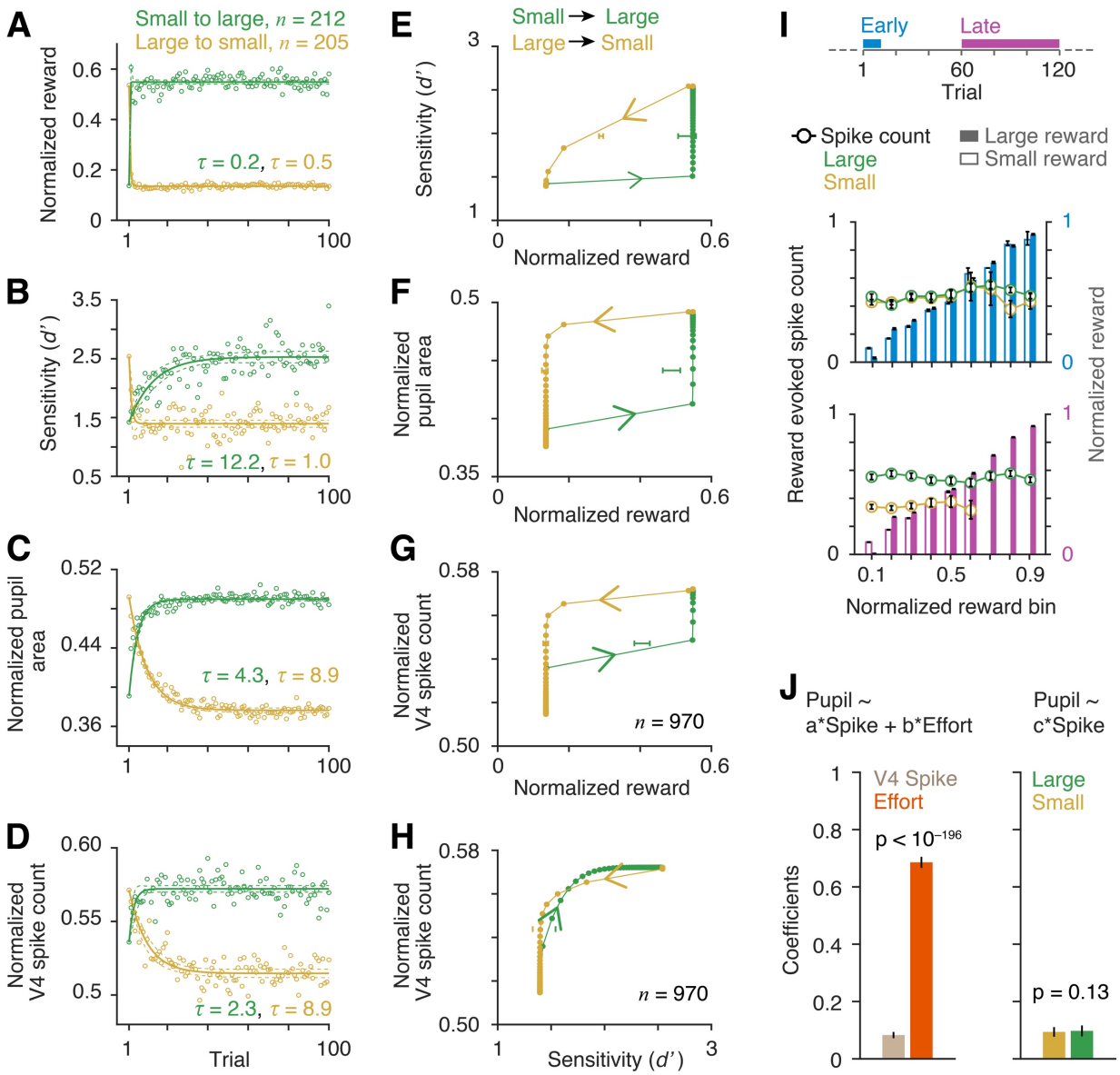

Figure 3. Directions of reward change have differential delayed effects on behavior and physiology. (**A-D**) Block averaged single received rewards (A), behavioral sensitivity (*d'*) (B), normalized mean pupil area during sample stimulus period (C) and normalized V4 spike counts across all neurons (n = 970; d) in large (N = 212) and small (N = 205) reward blocks. Circles, observed data. Lines, single exponential fits. τ, decay or rise constants. Trials are aligned with respect to the first correct trial following block transition. Dashed lines, 95% confidence intervals. (**E-G**) Hysteresis with transition of attentional effort. Behavioral *d'* (E), pupil area (F) and V4 spike counts (G) in response to reward changes from large to small and reverse. Horizontal error bars, mean ± SEM of reward size across blocks at the center value of y-axis variable. (**H**) V4 spike counts as a function of *d'* changes. Vertical lines, mean *d'* across blocks at the half-value of spike counts. (**I**) *Top*, Analysis widows for reward matched V4 spike counts in large and small reward blocks within first 10 trials at the beginning (*middle*, cyan) and last 60 trials at the end of blocks (*bottom*, purple). Bars, mean received rewards across trials binned between 0-1 (bin size = 0.2, overlap = 0.1; within session normalized) for two reward-block conditions. Error bars, 95% confidence intervals (bootstrap, $n = 10^4$). Circles, mean normalized spike counts (n = 970) on immediate next trial. (**J**) *Left*, Linear regression between mean pupil area (0 - 400

ms), spike counts (60 - 260 ms) and reward conditions (high and low efforts) across all trials were fit separately for each neuron. Population mean ± SEM of fitted coefficients (effort and spike counts) for neurons with significant fit ($p < 0.05$, $n = 625$). *Right*, Two separate linear regression fits between pupil area and spike counts for large and small reward trials. Mean ± SEM of fitted coefficients of spike counts in for the two reward conditions for neurons with significant fit ($p < 0.05$, $n = 334$).

173 However, the *d'* was much slower ($\tau = 12.2$) for transitions from small to large (**Figure 3B)**. As
174 expected, trial constants of percent-correct followed a time course similar to *d'* (large-to-small, τ
175 $= 1$; small to large, $\tau = 9.0$; **Figure S4**). In contrast to task performance, pupil area and population
176 mean V4 spike responses (60-260 ms from sample onset) had the same slow decays for large to
177 small transitions ($\tau = 9$ for both) and similar, faster rises for small to large transitions ($\tau = 4$ and 2
178 respectively for pupil area and spikes, **Figure 3C-D**).

179 The dynamics of the effects of reward transitions on neuronal firing, pupil area and
180 behavior can be clearly seen in hysteresis plots (**Figure 3E-G**). Behavioral *d'* tracks transitions
181 from small-to-large reward size more slowly than transitions from large-to-small reward size
182 (**Figure 3E)**. In contrast, pupil area and neuronal responses track transitions from small-to-large
183 reward size more quickly than transitions from large-to-small. The normalized reward value at
184 which the values reach their mid-point differ significantly for high-to-low and low-to-high
185 transitions for all three measures (horizontal bars in Figure 3E-G, mean ± SEM, $p < 10^{-31}$, t-test).
186 Similar neuronal hysteresis is also seen in motion perception and contrast detection in humans
187 where stimulus history affects perceptual detection threshold (Kleinschmidt et al., 2002; Williams
188 et al., 1986). The different dynamics between *d'* and spike rate were almost complementary
189 (**Figure 3H**), with spike rate leading for low-to-high transitions and lagging for high-to-low
190 transitions of *d'*.

191 While the average spike rate in area V4 changed slowly following block transitions, the
192 averages might obscure trial-to-trial changes in neuronal activity that tracked the reward received

193 on the previous trial. Because rewards for hits and correct rejections (CR) typically differed
194 (**Figure S1**), we could measure of dependency of spike counts on the previous reward. We sorted
195 trials into different bins depending on the normalized reward size on the preceding trial and
196 measured spike counts of each neuron (Methods). We further separated the trials based on whether
197 they occurred immediately after block transitions (within first 1-10 trials from the first correct
198 response after the reward switch) or during steady-state within a block (final 60 trials, 61-120)
199 (*top*, **Figure 3I**). Reward value on the previous trial did not affect spike counts [$F_{(8, 12801)} = 1.46$, p
200 = 0.164 for repeated measured factor reward value (9 levels); $F_{(1, 12801)} = 3.72$, p = 0.0537 for
201 between group factor, block-reward condition (large and small)] (*middle*, **Figure 3I**). The lack of
202 reward dependency of spike responses remained unchanged even during the late, steady state
203 portion of blocks (late trials), when a large effect of block-reward size was seen [$F_{(8, 10752)} = 1.18$,
204 p = 0.307 for reward value; $F_{(1, 10752)} = 7.78$, p = 0.005 for block-reward condition] (*bottom*, **Figure
205 3I**). Thus, the strong V4 response modulations we saw were dominated by slow effects.

206 The similar dynamics of pupil area (**Figure 3C**) and spike rate (**Figure 3D**) suggest that a
207 larger pupil area associated with high effort might enhance effective retinal illumination, which
208 might elevate V4 neuronal spiking. To test this possibility, we quantified how well pupil area
209 correlates with V4 spike rates and effort states ('high' or 'low') for all neurons using linear
210 regression (Methods). Regression coefficients for effort were more than eight-fold higher than the
211 coefficients for spike rate (mean ± SEM, spike rate, 0.08 ± 0.005; effort, 0.68 ± 0.01; Wilcoxon
212 rank sum test, (WRS) $n = 625$, $p = 10^{-196}$; **Figure 3J**, *left*). Weak relationship between pupil area
213 and spike rate was similar for the two reward conditions, when mean pupil area was fit separately
214 for small and large reward trials (mean ± SEM, small reward, 0.094 ± 0.008; large reward, 0.097
215 ± 0.01; WRS test, $n = 334$, p = 0.13; **Figure 3J**, *right*). We additionally measured the temporal
216 relationship between single trial V4 spike trains and pupil area dynamics using cross-correlation

217 and spike triggered averaged (STA) pupil area for each neuron (Methods). None of the neurons
218 show any significant correlation between PSTHs of pupil area and spike rates (binned at 10 ms)
219 over the analysis window from -350 ms to 350 ms from sample on (**Figure S6**). Similarly, STA-
220 pupil area that measured the extent to which individual spikes were aligned with pupil area did not
221 show any significant relationship between single spikes of individual neurons and pupil area
222 (absent of STA-pupil area >0 at negative lags; **Figure S7**). Together, these results suggest that V4
223 spike activity and the autonomic sympathetic system that regulates pupil dilation are both strongly
224 modulated by common top-down cognitive states rather than a direct influence of changing retinal
225 illumination on V4 spike activity within the limit of observed pupil area change.

226 **Encoding of attentional states in area V4**

227 To understand better how V4 neurons encode a cognitive state associated with enhanced
228 attentional effort, we fitted single trial spike counts of every neuron using a generalized linear
229 model (GLM) as a function of experimental predictor variables (Methods). In a detailed GLM
230 (complete model; **Figure 4A**), we used 13 predictor variables: orientation of sample stimuli inside
231 RF; mean pupil area during the sample period; the saccadic choice; and a reward history that
232 consisted of reward outcomes in each of the previous 10 trials. We also compared the performance
233 of this complete model with two reduced GLMs (**Figure S10**) that included either reward history
234 (reward model) or the pupil area (pupil model) alone (**Figure 4A**). Fitted single trial spike counts
235 in small and large reward conditions of an example neuron are shown in **Figure 4C**. Model
236 performance was measured by pseudo-R^2 values (Methods). Most neurons (78%, 757/970) were
237 significantly fit ($p < 0.05$, F test) with the complete model. Fewer neurons had significant fits for
238 the reduced models (reward model, 12%, 114/970; pupil model, 50%, 483/970; **Figure 4B**).
239 **Figure 4D** shows population averaged spike counts of all fitted neurons estimated from the
240 complete GLM with overlying observed responses. We next compared the relative contributions

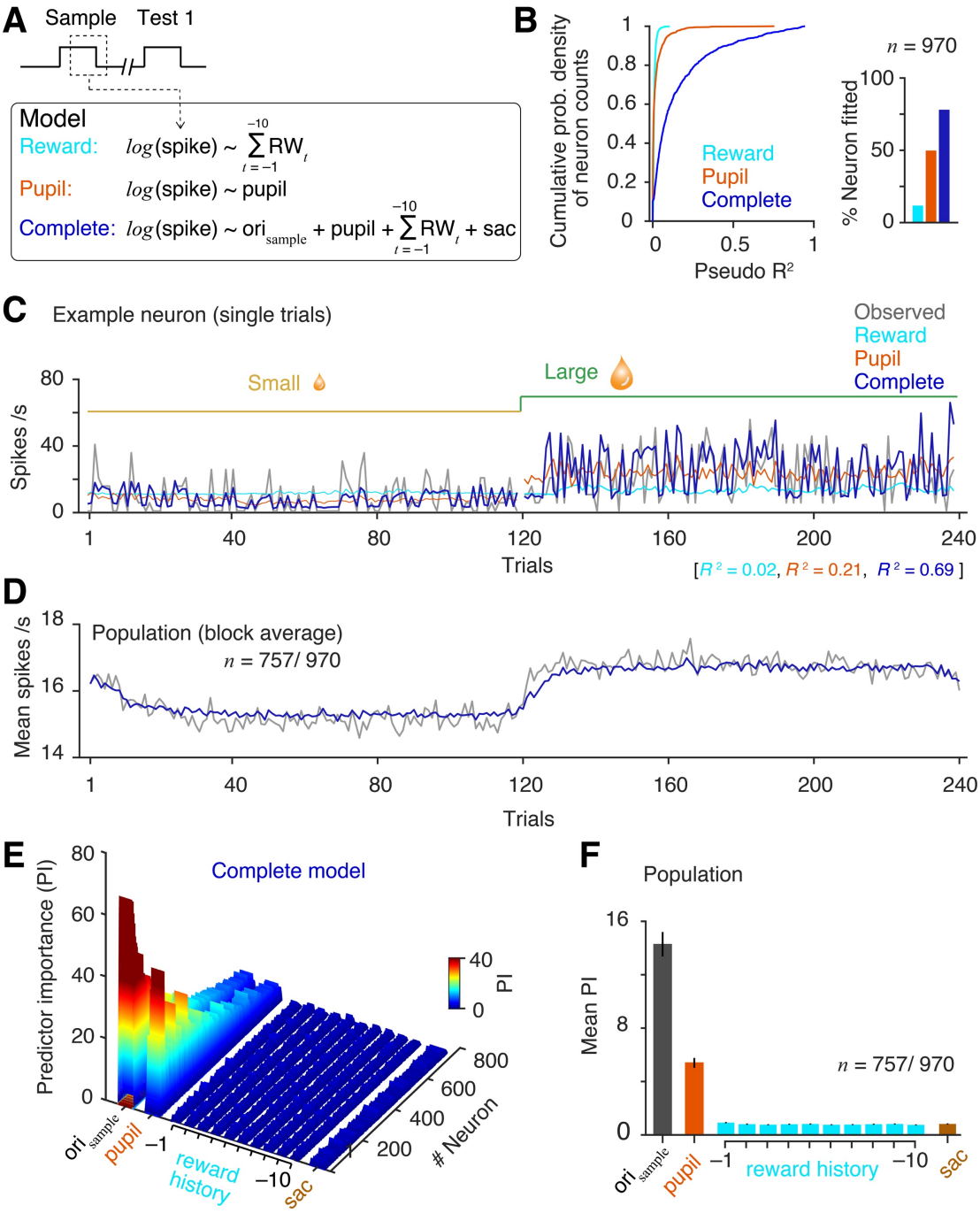

Figure 4. Encoding of cognitive states by single trial spike counts. (**A**) *Top*, Generalized linear models (GLM) on single trial spike counts during sample stimuli period (60 - 260 ms from sample onset). Spike counts were fit with three different GLMs. Two were reduced models, based on either reward history (10 immediate past received rewards; reward model) or mean pupil area over 400 ms following stimulus onset (pupil model). A more detailed model contained multiple experimental and cognitive state variables that included reward history (past 10 trials), pupil area, saccade response and Gabor stimulus orientation (complete model). (**B**) *Left*, Cumulative probability densities of pseudo R^2 values (Methods) of single

241

neurons measure goodness of fit for different GLMs. *Right*, fraction of the neuron population that were fitted significantly better ($p < 0.05$, F test) compared to a null model (a constant) [reward model, 114/ 970 (12%); pupil model, 483/ 970 (50%); complete, 757/ 970 (78%)]. (**C**) Observed and model predicted spike counts on single trials from cross-validation test-dataset for an example neuron in two representative reward blocks. (**D**) Population averaged observed and fitted (complete model) spike counts. Gray, observed; blue, complete model. (**E**) Comparing predictor importance (PI) that measures contributions of different predictor variables estimated by absolute standardized predictor coefficient values. Colormap represents PIs of all neurons that were fitted with the complete model ($n = 757$). Neurons were sorted based on the pseudo R^2 values. (**F**) Population averaged PIs. Error bars, 95% confidence intervals (bootstrap, $n = 10^4$).

of the experimental variables on spike responses for each neuron as measured by predictor importance (PI), which is the normalized magnitude of fitted coefficients (Methods). Stimulus orientation has the strongest contribution to the spike counts, which is expected because most V4 neurons are orientation selective (PIs of individual neurons, **Figure 4E**; mean PI across neurons, **Figure 4F**). More interestingly, single trial pupil area (a physiological proxy of attentional effort) also strongly predicts spike response compared to reward history and saccade choice. Instantaneous pupil area remained a strong predictor when we compared with constant effort levels ('high' and 'low') as well as block-averaged single trial pupil area in two alternate models (PI, mean ± SEM, constant effort, 2.3 ± 0.07; blocked-averaged pupil area, 2.7 ± 0.09, instantaneous pupil area, 5.37 ± 0.19; ANOVA, $F_{(2, 2195)} = 166.31$, $p < 10^{-67}$; **Figure S11**). Together, these suggest that even though reward history is the primary external motivator for the monkeys, V4 spike responses to the sample stimuli encode instantaneous attentional effort more strongly than recent reward outcome value or saccade choices.

It is possible that reward history has more weight around the time of block transitions, when expectations change rapidly (Baruni et al., 2015). Because most of the trials within blocks in our task occur long after a transition (steady-state), this weight would be diluted. To address this, we also fit spike counts from only the first 20 trials after block transitions with the same complete-GLM as shown in Figure 4A. (**Figure S12**). As with the complete data set, stimulus orientation and pupil area contribute much more strongly to V4 spike counts than does reward history.

261 Although both the pupil area and spike counts are not directly related, they are linked to the top-
262 down attentional effort in a similar way. Thus, the attentional state as represented by pupil area is
263 encoded on single trial spike counts during the sample stimuli period.

264 **Dynamic encoding of stimulus change-detection in area V4**

265 Although reward representation in V4 is weak during the sample stimuli interval, stronger signals
266 might emerge closer to the behavioral response. We therefore separately fit spike counts during
267 the choice interval (test 1 interval) using a similar complete GLM. We used only those trials for
268 which test 1 stimulus appeared inside RFs and the animal did not initiate a saccade until after the
269 analysis period (which was 60-260 ms from test 1 stimulus onset; 44.4% (22238/50038) of the
270 trials) (**Figure S13**). The stimulus feature variable in this model was the product of orientation
271 tuning filter and test 1 stimulus orientation, as there were four different orientations of test 1
272 stimulus. The remaining variables were mean pupil area during the test 1 presentation, reward
273 outcomes in each of the previous 10 trials and the saccadic choice.

274 Reward history remained a poor predictor of single trial spike counts compared to pupil
275 area (**Figure S13**). Notably, the saccade choice variable is also a strong predictor of spike
276 responses for the same neuronal population. Previous reports have shown that spike responses of
277 V4 neurons enhance before initiating a saccade towards the RF location(Burrows et al., 2014;
278 Moore et al., 1998). Among all the saccade sensitive neurons (n = 256, significant saccade
279 coefficient, $p < 0.05$) about two-thirds were more active before saccades (saccade-preferred
280 neurons; saccade coefficient > 0; n = 149/ 256) and the rest were less active (saccade-anti-preferred
281 neurons, saccade coefficient < 0; n = 107/ 256). Further, based on behavioral outcomes (hit, miss,
282 CR and FA), we sorted observed spike counts on single trials during sample and test 1 stimulus
283 periods for these two neuron types, saccade preferred and saccade anti-preferred (**Figure S13**). A
284 true encoding of saccade choice by these neurons predicts indistinguishable spike response

between hits and FAs (and between CRs and misses). Instead, spike responses of saccade preferred neurons increase for hits and misses (nonmatch trials) compared to CRs and FAs (match trials). Similarly, responses of saccade anti-preferred neurons increase for CRs and FAs (match trials) compared to hits and misses (nonmatch trials). This suggests that saccade choice is not a suitable predictor variable in accounting single trial spike counts during the test 1 interval; rather 'stimulus orientation-change' can be a better predictor parameter.

We next fit the same dataset of spike counts during test 1 stimulus with a complete-GLM as mentioned above except, the saccadic choice variable was replaced with stimulus orientation change (Δori) (*top*, **Figure 5A**). The variable Δori represents the trial type: match or non-match trial. Covariance between single trial absolute test 1 stimulus orientation and Δori is small (mean partial correlation 0.005) across sessions due to small Δori values (16°-32°). Further, we used only the neurons with very weak correlation coefficients (< 0.2) between model-predicted spike counts due to stimulus feature (product of orientation tuning filter and test 1 orientation) and Δori to rule out stimulus orientation-related effects on estimates of Δori coefficient. V4 spike counts robustly encode information of single trial Δori (**Figure 5A-B**). Based on significant Δori coefficients ($p < 0.05$), two populations of neurons were classified, Δori-preferred (Δori coefficient > 0, n = 130/ 521) and Δori anti-preferred (Δori coefficient < 0, n = 109/ 521). As expected, orientation change differentially modulates mean spike counts during the test 1 interval in these two neuron subpopulations in accordance with the change in stimulus orientation [two factor repeated measured ANOVA, $F_{(1, 237)} = 15.33$, $p = 10^{-4}$ for neuron types (Δori preferred, Δori anti-preferred); $F_{(3, 711)} = 7.83$, $p < 10^{-4}$ for repeated measured factor response choices (hit, miss, CR and FA)] (*right*, **Figure 5C**).

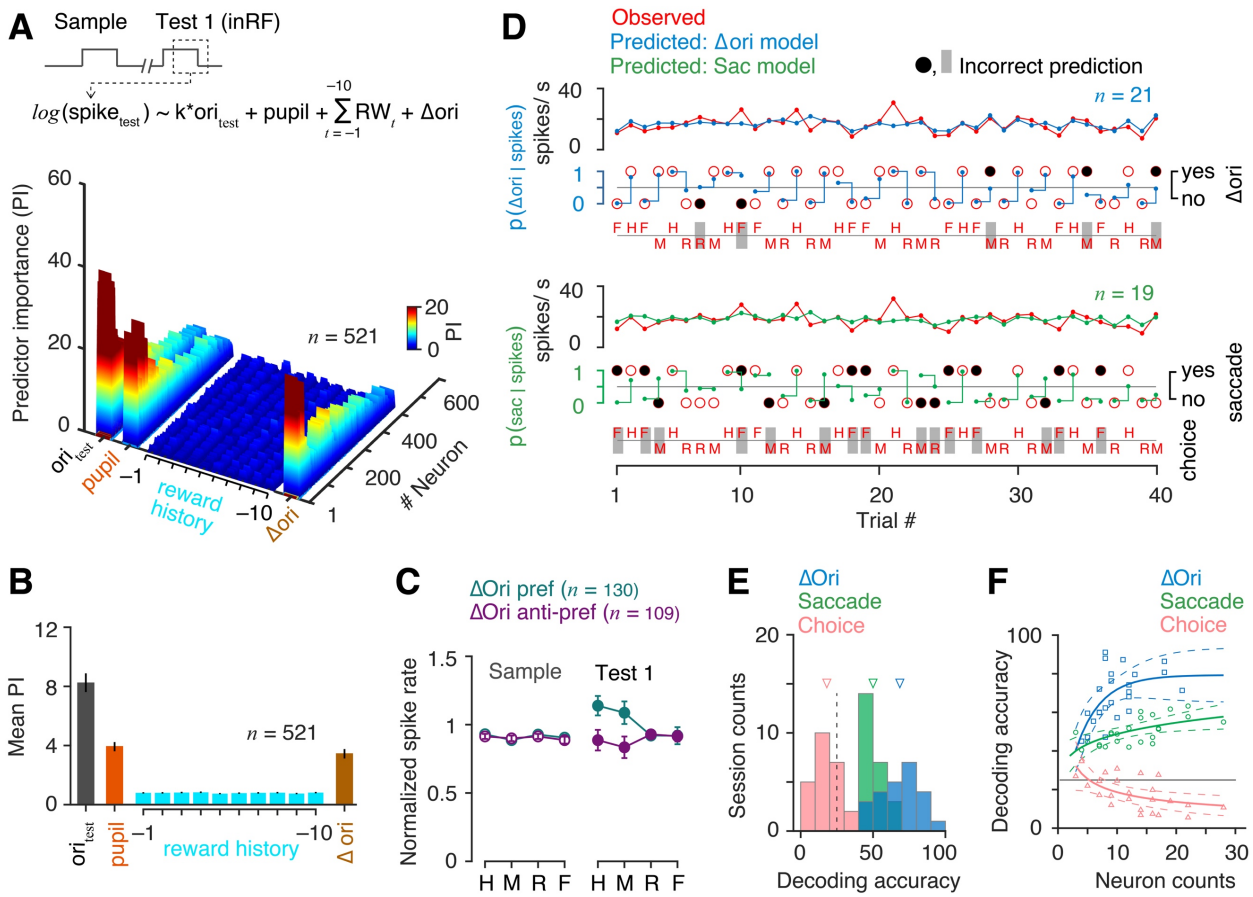

Figure 5. V4 spikes encode change in stimulus orientation immediately prior to response selection. (**A**) *Top*, Δori model: GLM of spike counts during test 1 interval (60-260 ms from test 1 on). Predictor variables: product of test 1 stimulus orientation and neuron's orientation tuning filter, pupil area, reward history and orientation change (match or nonmatch trial). Only the trials when test 1 stimulus appeared inside RF of recorded neurons and monkey did not initiate any saccade before analysis period (44.4% of the total trails). *Bottom*, Contributions of predictor variables to spike counts of single neurons. (**B**) Population averaged predictor importance ($n = 521$). (**C**) Observed normalized mean V4 spike rates of Δori responsive neurons during sample and test 1 stimulus presentations for different behavior choice trials. H: hit, M: miss, R: correct rejection, F: false alarm. Neurons with significant Δori coefficient ($p < 0.05$) are classified as Δori-preferred (coefficient < 0, $n = 130$) or Δori-anti-preferred (coefficient < 0, $n = 109$) based on the GLM fits. (**D**) Decoded task variables on randomly selected pair of trials from cross-validation test-dataset in an example session. GLM fitted coefficients and observed single trial V4 spike counts are used to estimate probability of Δori (Δori model, Figure 5A) and probability of saccade (saccade model, Figure S11). Open red circle, observed response. Filled black circles, incorrect prediction. Dot, predicted probability of a response. (**E**) Decoding accuracy of response choice, saccade and Δori for cross validation test datasets across all sessions (N = 24) using GLM fits. Triangles, population means. Dashed line, 25% chance level. (**F**) Decoding accuracy as a function of number of neurons used for decoding across sessions ($N = 24$). Markers, individual session. Solid lines, second order polynomial fits. Dashed lines, 95% confidence intervals. Error bars, 95% confidence intervals.

307

308 Finally, we tested the detection accuracy of stimulus orientation change from observed V4 spiking
309 activity during the test 1 stimulus by using the fitted model on a single trial in a 10-fold cross-
310 validation test dataset (Methods). A random pair of trials, one from non-match (hit or miss) and
311 another from match (CR or FA) without replacement, were selected. For each of these two trials,
312 we evaluated the likelihoods of observed spike counts to be consistent with spike counts under the
313 two possible orientation changes for each fitted neuron within a session. Sum of the log-likelihood
314 ratios across neurons amounts to the predicted probability of a realization of orientation change on
315 that trial. Only if the decoded orientation changes on both trials of the selected pair match with the
316 observed data was the discrimination of an orientation-change from no-change considered correct.
317 **Figure 5D** shows model-fitted population-averaged spike counts and decoded task variables,
318 orientation change (*top*, using Δori GLM) and saccadic choice (*bottom*, using saccade GLM as
319 described in Figure S11) on 20 pairs of randomly selected trials in an example session. Similar to
320 saccade prediction, we also tested accuracy in discriminating response choices i.e. hit from miss
321 or FA from CR from observed spike counts during test 1 using the same saccade-GLM. Prediction
322 accuracy of orientation change (using Δori-GLM) is better than both saccade and choice (hit vs
323 miss or CR vs FA) predictions (using saccade-GLM) across all sessions (mean ± SEM, Δori, 68.5
324 ± 2.8%, saccade, 50.0 ± 1.4%, choice, 18.1 ± 1.8%; $p = 10^{-25}$, $F_{(2,69)} = 154.2$, ANOVA; **Figure**
325 **5E**). Decoding performance of Δori is better compared to saccade irrespective of the number of
326 neurons used for decoding within a session (**Figure 5F**). Together, these encoding and decoding
327 models offer powerful methods in isolating task relevant variants and reading out perceptual or
328 decision signals from a population of neuronal spikes.

DISCUSSION

We found that isolated changes in attentional effort modulate the activity of neurons in V4. Previous reports on effort-related modulation in V4 (Boudreau et al., 2006; Spitzer et al., 1988) conflated changes in effort with changes in attentional selectivity (how much one location is favored over others), which strongly modulates V4 neuronal activity (Cohen and Maunsell, 2009; Luo and Maunsell, 2015; Moran and Desimone, 1985; Reynolds and Heeger, 2009). Compared to previous results, the current data is the first demonstration that V4 neurons are modulated to a comparable degree by either non-selective attentional effort or attentional selectivity. As a result of reward size changes, the block averaged cortical responses covary with physiological pupil area and behavioral performance (*d*'). However, these three measures dissociate at the block transitions and exhibit differential degrees of dependency on trial history. Stimulus features and pupil area strongly contribute to V4 spike counts throughout the trial duration as revealed by single trial information encoding. V4 spike counts contain very little information about immediate reward history. Additionally, perceptual detection of a task-relevant stimulus emerges as a strong contributor to V4 spiking during the decision period. This perceptual detection is independent of behavioral choice.

The rise of *d'* following an increase in reward is slow relative to the increase in V4 spike rate and pupil area. This may occur because performance in an attention demanding task depends not only on the state of sensory structures such as V4, but also on that in downstream decision and motor circuits. These downstream circuits could respond to changes in reward with their own dynamics. It remains to be determined how much subjects can control the dynamics of their responses to changes in reward expectation. Our design used no cueing other than reward size itself. It is possible that an explicit cue at the beginning of each trial might produce more coincident changes in neuronal spiking and *d'*. However, animal subjects typically achieve less pronounced

353 behavioral changes when trials of different reward contingencies are randomly interleaved on each
354 trial, and spatial cues at the start of the trial indicate the trial type (Baruni et al., 2015). Block-wise
355 control of animals' effort can be more effective for producing performance changes. Although a
356 limitation of the latter design is that the reward outcome and attentional state covary and make it
357 more challenging to dissociate true representation of neuronal modulation (for review (Maunsell,
358 2004)). Our task design of manipulating attentional states within small block of trials and using
359 single trial analysis was crucial for isolating relative contributions of attentional effort, reward
360 history and perceptual performance.

361 In contrast to reward increase, performance drops quickly with decreased reward even
362 though pupil area and neuronal response remain elevated (i.e. delayed decay, **Figure 3**). Dissimilar
363 effects of reward change directions on behavior are often seen across species (Kimchi and
364 Laubach, 2009; Saez et al., 2017). Independence of V4 neuronal activity from single trial
365 behavioral performance is consistent with the notion that transitions between states occur with
366 different dynamics in downstream structures that read out perceptual detection and weigh
367 anticipated outcomes against the cost of initiating and executing action (Baruni et al., 2015; Zénon
368 and Krauzlis, 2012).

369 The observed hysteresis in V4 spike responses with reward changes represents a form of
370 memory. Hysteresis at the input-output level of a single neuron can improve memory capacity and
371 retrieval properties in the presence of noise in a synchronous network of neurons with nonlinear
372 threshold (Wang and Ross, 1990). Indirect evidence of hysteresis in single cortical neurons comes
373 from the fact that spike train history is an important predictor of individual spikes (Park et al.,
374 2014; Pillow et al., 2008). Spike counts on reward-matched trials are indistinguishable between
375 the two reward conditions immediately after the reward switch and become different only in later
376 trials when the animal's effort attains a steady level (**Figure 3I**). These results together with

377 reward-spike hysteresis (**Figure 3G**) strongly support a dependency of V4 neuronal activity on
378 history of attentional effort state. Previous trial history of task relevant signals has also been
379 reported to strongly modulate PFC neurons (Donahue and Lee, 2015). Neuronal hysteresis during
380 visual perception has been suggested to arise from cooperativity between interconnected neurons
381 (Williams et al., 1986; You et al., 2011). Future experiments are required to dissociate the role of
382 single cell excitability and connectivity among neurons on neuronal hysteresis in V4. Absence of
383 reward modulation (immediate past trial outcome) of spike counts on reward-matched trials in
384 trials immediately after block transitions is inconsistent with immediate reward representation as
385 reported in previous studies (Baruni et al., 2015; Cicmil et al., 2015). Like V4, many other brain
386 areas show correlated spike activity with pupil area, including structures implicated in
387 attention(Joshi et al., 2016). A noradrenergic neuromodulation of V4 neurons might mediate such
388 brain-wide attentional state representation.

389 The relationships between reward expectation, behavioral d' and V4 spiking have also been
390 examined in a previous study (Baruni et al., 2015) that found the expectation of a large reward
391 increases spike rates of V4 neurons relative to expectation of a low reward, even when d' is the
392 same across those conditions. Consistent with this previous finding, we found that the d' was
393 slower to respond to changes in reward schedule than was V4 spiking. The early study randomly
394 interleaved different rewards conditions on a trial-by-trial basis, while our task contingencies were
395 entirely predictable over blocks of 120 trials. We would expect to see results qualitatively similar
396 to the previous report (Baruni et al., 2015) if we randomly interleaved trials. Unlike previously
397 observed positive correlation between absolute reward size expectation and V4 spiking (Baruni et
398 al., 2015), we found very weak representation of reward history in single-trial V4 spike counts
399 using both reward-matched spike count analysis and GLM-based encoding model, even
400 immediately after block transitions when the knowledge of reward expectancy was crucial for

401 guiding behavior. In our study, the reward on each trial varied around a mean within each reward
402 schedule (**Figure S1),** whereas a fixed reward was used for a given reward-schedule in the earlier
403 study. Our additional reward-variance provided negligible covariances between reward size and
404 other task variables, and was crucial for reliable isolation of multiplexed information on single-
405 trials using GLM. Prior application of GLM-based encoding in primate cortical areas has identified
406 dependencies of correlated spikes on multiplexed sensory, cognitive and motor signals (McGinty
407 et al., 2016; Park et al., 2014). Performance of our model fit can be further improved by taking
408 into account of spike history or interaction with other units within the network (Park et al., 2014).
409 Previous studies have described that V4 spiking increased when an animal intends to make
410 a saccade towards the neuron's RF (Burrows et al., 2014; Fischer and Boch, 1981a, b; Moore et
411 al., 1998). However, single trial encoding shows that the observed correlation between V4 spike
412 counts and saccade initiation is primarily due to perceptual signal detection and not saccade
413 preference. Spike rate (Shiozaki et al., 2012) and pairwise noise correlation (Cohen and Maunsell,
414 2009) between spike counts of V4 neurons have been suggested to represent a detection threshold
415 and predict choice probability in perceptual discrimination tasks. Ablation of V4 has revealed no
416 effects on saccade amplitude or latency to visual targets (Schiller and Lee, 1994). In partial
417 agreement with some of these findings, our results confirm the role of V4 in single trial perceptual
418 detection but rejects a direct contribution to saccade choice. High covariance between perceptual
419 detection and behavioral choice in previous tasks may have limited the detailed isolation of
420 information coding of perception from decision. In the present study, we identified two types of
421 response populations in V4 that are differentially modulated with perceptual signal changes. Future
422 work at the microcircuitry level is required for detailed characterization of these two cell
423 populations with respect to their inputs and recurrent connections. Understanding the finer
424 dynamics of cognitive task variants within a single trial would require modeling at the time scales

425 of single spikes (Park et al., 2014). A perceptual task with a continuous stream of visual stimuli
426 would be ideal to evoke a sufficient number of spikes throughout the task period for studying
427 visual areas like V4 that have low activity in the absence of visual stimulation. Overall, our
428 experimental framework provides new evidence revealing information encoding of higher brain
429 function that can be extended to other brain areas.

430 METHODS

431 Subjects and surgery

432 All experimental procedures were approved by the Institutional Animal Care and Use Committee
433 at the University of Chicago and were in compliance with US National Institutes of Health
434 guidelines. Two adult male rhesus monkeys (*Macaca mulatta*, 13 and 9 kg) were implanted with
435 a titanium head post using aseptic surgical techniques before training began. After the completion
436 of behavioral training (3 to 5 months), we implanted an 10x10 array microelectrodes with 400 μm
437 spacing (Blackrock Microsystems) into dorsal visual area V4 of one hemisphere, between lunate
438 and superior temporal sulci.

439 Behavioral task

440 During training and neurophysiological recording, the monkey was seated in a primate chair facing
441 a calibrated CRT display (1024 x 768 pixels, 100 Hz refresh rate) at 57 cm viewing distance inside
442 a darkened room. Binocular eye position and pupil area were recorded at 500 Hz using an infrared
443 camera (Eyelink 1000, SR Research). Trials started once the animal fixated within 1.5° of a central
444 white spot (0.1° square) presented on a mid-level gray background (**Figure 1A**). The animal had
445 to maintain fixation until its response at the end of the trial. After a fixation period of 400-800 ms,
446 two achromatic Gabor sample stimuli appeared for 200 ms, one in each visual hemifield. After a
447 variable delay of 200-300 ms, a Gabor test stimulus (test 1) appeared for 200 ms at one of the two

448 target locations, randomly selected with equal probability. The test stimulus was identical to the
449 preceding sample stimulus, except for its orientation. On half of the trials, the test 1 stimulus had
450 a different orientation (nonmatch trial) and the monkey had to make a saccade to that target
451 location to receive an apple juice reward. On the remaining half of the trials, the test 1 stimulus
452 had the same orientation as the corresponding sample stimulus (match trial), and the monkey had
453 to maintain fixation until a second test stimulus with a different orientation (test 2, 200 ms)
454 appeared in the same location after an additional delay interval of 200-300 ms. The monkey then
455 had to saccade to that target to get a reward. Inter-trial intervals varied from 2-3 s. Stimuli were
456 presented always in the lower hemifields at 2°-4° eccentricity. Gabors were odd-symmetric with
457 the same average luminance as the background. Spatial frequency, size and base orientation of
458 Gabor stimuli were optimized for one neuron recorded each day, and remained unchanged
459 throughout each session (left, azimuth -2.5^{o} to -5.3^{o}, elevation 0.0^{o} to -3.5^{o}, sigma, 0.35^{o} to 0.60^{o},
460 spatial frequency 0.6 to 3.5 cycles/^{o}; right, azimuth 2.8^{o} to 5.5^{o}, elevation 0.0^{o} to -2.5^{o}, sigma,
461 0.40^{o} to 0.65^{o}, spatial frequency 0.7 to 3.0 cycles/^{o}). On every trial, the orientation of the sample
462 stimuli randomly took one of two values, base orientation or orthogonal. Orientation change
463 (difficulty) remained fixed within a session and varied across sessions between 24°-32° for monkey
464 S and 16°-20° for monkey P.

465 Attentional effort was controlled over blocks of trials by changing reward volumes for
466 correct responses over a 4-5-fold range. Every 120 trials, reward size alternated between large and
467 small values without any prior cue to the animal. Reward sizes for hits (correct response in
468 nonmatch trial) and CRs (correct rejections in match trial) were adjusted as needed to encourage
469 the animal to maintain a behavioral criterion close to zero(Luo and Maunsell, 2015). Although,
470 trial averaged criterion within a reward condition remained zero, there was a transient change in

criterion immediate after the block transition (reward switch) which then approached zero over a few trials (**Figure S5**). Distributions of reward sizes are shown in **Figure S1**.

Electrophysiological Recording and Data Collection

Extracellular neuronal signals from the chronically implanted multielectrode array were amplified, bandpass filtered (250–7,500 Hz) and sampled at 30 kHz using a Cerebus data acquisition system (Blackrock Microsystems). We simultaneously recorded from multiple single units as well as multiunits (563, monkey S; 407, monkey P) over 24 sessions (15 for monkey S, 9 for monkey P). Before each experimental session, we mapped receptive fields and stimulus preferences of neurons while the animal fixated. These fields were used to optimize the stimulus parameters. Spikes from each electrode were sorted offline (Offline-Sorter, Plexon) by manually defining cluster boundaries using principal component as well as waveform features. Well isolated clusters based on J3 statistics were classified as single units (Nicolelis et al., 2003). J3 measures the ratio of the average distance between points within clusters to the average distance between clusters. It takes a maximum value for compact, well-separated clusters.

Data Analysis

Behavioral performance

All completed trials (120 trial per block) were included in our analysis. Behavioral sensitivity (*d'*) and criterion (*c*) were measured from hit rates within nonmatch trials and FA rates within match trials as:

$$d' = \Phi^{-1}(hit\ rate) - \Phi^{-1}(FA\ rate) \quad (1)$$

$$c = -\frac{1}{2}[\Phi^{-1}(hit\ rate) + \Phi^{-1}(FA\ rate)] \quad (2)$$

where Φ^{-1} is inverse normal cumulative distribution function. We measured average *d'* and *c* within a session across all trials for large- and small-reward blocks separately. To examine the

494 dynamics of *d'*, *c*, and percent-correct at i^{th} trial (i = 1 to 120), we measured block averaged values

495 for each reward conditions. Overall *d'* was measured by,

496 $$d'_{overall} = \sqrt{(d'^2_{InRF} + d'^2_{OutRF})} \quad (3)$$

497 Where, d'_{InRF} and d'_{OutRF} are the sensitivities in the two hemifields, inside and outside the recorded

498 neurons' receptive fields.

499 ***Pupil area***

500 All pupil area measurements were measured binocularly at 500 Hz while monkeys maintained

501 fixation in absence of a luminosity change using infrared camera (EyeLink 1000, SR Research).

502 Raw pupil areas were normalized for each session and each eye separately. Mean pupil area was

503 measured by averaging the normalized pupil area over 400 ms from sample appearance.

504 ***Neuronal response***

505 Only neurons with an average spike rate 60-260 ms after sample stimulus onset that was

506 significantly ($p < 0.01$) greater than the rate 0 to 250 ms before sample onset were used in the

507 analysis. To construct peri-stimulus time histograms (PSTHs) for figures, spike trains were

508 smoothed with a half Gaussian kernel (15 ms SD with only a rightward tail), aligned to sample

509 stimuli onset and averaged across trials. A spike rate modulation index (MI) for each neuron was

510 calculated as the difference in average spike counts (60–260 ms after sample onset) between large

511 and small reward blocks (correct trials) divided by their sum.

512 $$MI = \frac{\langle Spike\ count_{large}\rangle - \langle Spike\ count_{small}\rangle}{\langle Spike\ count_{large}\rangle + \langle Spike\ count_{small}\rangle} \quad (4)$$

513 For analyzing trial-by-trial dynamics of spike counts and GLM, absolute spike counts within 60 to

514 260 ms from sample stimuli onset (or test 1 onset) were used.

515 Principal component analysis (PCA) was done on spike rates from 0-400 ms separately for

516 each monkey in Matlab. Each neuron had two spike rates, one each for one type of reward block

517 (small or large reward). For monkey P, there were 407 neurons (814 spike trains) and for monkey
518 S, there were 563 neurons (1126 spike trains). Linear regression was fitted between PC scores of
519 spike histograms in small and large reward blocks for the first three principal components.

520 ***Pupil area-spike count-effort linear regression***

521 Average pupil area over 0-400 ms from sample onset and spike counts from 60-260 ms on each
522 individual trial were used for linear regression analysis for pupil area *versus* spike count and
523 average effort states ("low" and "high") (**Figure 3J**, *left*). The pupil area was modeled as: *pupil*
524 *area* ~ *a**(*spike count*) + *b**(*effort*). Where *a* and *b* are the regression coefficients. All the trials
525 across small and large reward conditions that occurred after the first correct response (hit or CR)
526 following the reward switch were included in the analysis. In a second model: *pupil area* ~
527 *a**(*spike count*), each neuron was fitted separately for two reward conditions, small and large
528 (**Figure 3J**, *right*). For this model, we used a subset of trials with matched pupil areas between the
529 two reward conditions. Standardized coefficients were compared across neurons that were fit at
530 significant level of $p < 0.05$ (F-test).

531 ***Pupil area-spike count cross-correlation***

532 We measured cross-correlations between two time series, spike rates and pupil area as a function
533 of time lag over 700 ms period around the sample stimulus on (–350 ms to 350 ms) for each neuron.
534 Single trial spike trains were binned in a 10 ms sliding window (2 ms increments) and converted
535 to spike rates. Pupil area time series was sampled at 500 Hz and directly used for the cross-
536 correlation analysis. Single trial cross-corrrelations were averaged, and trial-shuffled values were
537 subtracted separately for trials with small and large reward conditions.

538 ***Spike triggered averaged pupil area***

539 We measured a spike triggered averaged (STA) pupil area for each neuron within a time window
540 of 0-400 ms from sample stimulus onset, across all trials. The time series of pupil areas were

541 aligned to individual spikes, and averaged. Finally, trial-shuffled subtracted STA was subtracted
542 from this averaged STA-pupil area for each neuron.

543 ***Generalized linear model (GLM)***

544 Generalized linear model (GLM) regression was used to estimate the relationship between single
545 trial spike responses and reward expectancies, attentional efforts, behavior choices and stimulus
546 parameters. Single trial stimulus evoked spike counts were modeled to follow a negative binomial
547 distribution. The negative binomial distribution is well suited for the purpose, as spike count
548 variances of cortical neurons are most often equal to or greater than their means (**Figure S8**)
549 (Churchland et al., 2010; Shadlen and Newsome, 1998). Reward expectancy was represented by
550 reward history on 10 trials preceding the trial being considered. Mean pupil area during 400 ms
551 following stimulus onset served as a proxy for attentional effort. A categorical saccade choice
552 variable could take two values: saccade (hit and FA) or no saccade (CR and miss). For fitting of
553 test 1 spike counts, an alternate categorical task variable "stimulus orientation change" (Δori) was
554 used instead (**Figure 5A**). This perceptual variable had two values: orientation change (nonmatch
555 trial) or no orientation change (match trial). The product of the absolute orientation of Gabor
556 stimulus and neuron's orientation tuning filter served as a test 1 stimulus feature variable. There
557 were four different orientations of test 1 stimulus. There were no correlations (partial) among
558 predictor variables (**Figure S9**). For the GLMs on test 1 spikes, in addition to the predictor variable
559 covariances, we also cross checked the correlation between model predicted spike counts due to
560 test 1 stimulus feature and Δori in order to isolate the orientation-tuning related effect on the
561 perceptual variable Δori. We considered only the neurons that showed correlation (Spearman) of
562 <0.2 for further analysis.

For a sample y_1, y_2,....,y_n of independent response variable y from an exponential family, there exists a linear predictor $\beta_0 + \beta_1 x_1 + \ldots + \beta_k x_k$ of the response variable y. The mean response $\left(\mu_y = E[y|x_1, .., x_k]\right)$ depends on the linear predictor through a link function $g(\cdot)$:

$$g\ (\mu_y) = \beta_0 + \beta_1 x_1 + \cdots + \beta_k x_k \tag{5}$$

Where, x_j (j = 1,2,…,k) is a set of independent predictor variables. Assuming that the spike count responses in non-overlapping time intervals are independent and variance is equal or greater than (over dispersion) the mean, they can be modeled as negative binomial variables. As the mean spike count is always positive, it can be modeled as:

$$\mu_y = exp\ (\beta_0 + \beta_1 x_1 + \cdots + \beta_k x_k) \tag{6}$$

The probability density function for a random variable for which there are y successes of Bernoulli trials until θ^{h} failure occurs follows a negative binomial distribution:

$$P\left(y; \mu_y, \theta\right) = \frac{\Gamma(y+\theta)}{\Gamma(\theta) y!} \frac{{\mu_y}^y\ \theta^\theta}{(\mu_y+\theta)^{y+\theta}} \tag{7}$$

with a mean μ_y and variance $V(y)$:

$$\mu_y = \frac{\theta p}{1-p} \tag{8}$$

$$V_y = \mu_y + \frac{{\mu_y}^2}{\theta} \tag{9}$$

where, p is probability of success of each Bernoulli trial. 1/θ is the dispersion parameter (θ *is* also called as shape parameter). Γ is gamma distribution. The likelihood for a negative binomial random variable y_i (i = 1,2,…,n) that depends on a set of k predictors of $x_{i,j}$ (j = 1,2,…,k):

$$L(P) = \prod_{i=1}^{n} \frac{\Gamma(y_i+\theta)}{\Gamma(\theta)\ y_i!} \frac{{\mu_{y_i}}^{y_i}\ \theta^\theta}{\left(\mu_{y_i}+\theta\right)^{y_i+\theta}} \tag{10}$$

The log-likelihood is:

$$LL(\beta_0, \beta_1, \ldots, \beta_k, \theta) = log\ \left(L(P)\right) \tag{11}$$

The predictor coefficients β_j (j = 1,2,…,k) and shape parameter θ are obtained from maximum likelihood estimates by solving:

$$\frac{\partial LL}{\partial \beta_j} = 0,\ j = 1,2,\dots,k \tag{12}$$

$$\frac{\partial LL}{\partial \theta} = 0 \tag{13}$$

GLM was implemented in Matlab separately for each neuron. In order to compare different predictor coefficients, they were converted post-hoc into standardized coefficients:

$$\beta_j{}' = \beta_j * \frac{\sigma_y}{\sigma_x},\ j = 1,2,\dots,k \tag{14}$$

Standardized coefficient corresponds to the *log* ratios of the mean responses (in units of standard deviation) due to one standard deviation change in the predictor variable, holding all other variables constant.

<u>Goodness of GLM fit and model comparison:</u> Goodness of fit for a given GLM was measured by residual deviance (D) and pseudo R-squared (Cragg & Uhler's method) value. Residual deviance measures how close the predicted values from the fitted model match the actual values from the raw data:

$$D = 2[LL(saturated\ model) - LL(model)] \tag{15}$$

The saturated model comprises a model for which the number of parameters equals the number of samples. Thus, the predicted response in the saturated model is same as the observed response. Deviance measures lack of fit in maximum log-likelihood estimations similar to the residual variance in ordinary least square methods. The lower the deviance, better is the model fit. For a large sample size and small deviance, it approximately follows chi-square distribution of n–k–1 degrees of freedom. A statistic that indicates value of a proposed model is based on how well the model predicts data compared to a null model having a single predictor β_0:

$$\chi^2 = D(null\ model) - D(model) \tag{16}$$

$$= 2[LL(model) - LL(null\ model)] \tag{17}$$

The test statistic χ^2 follows an approximate chi-square distribution of degrees freedom *n–k*. We tested at a level of significance $p < 0.05$.

As the ratio of the likelihoods reflects the improvement of the proposed model over the null model (the smaller the ratio, the greater the improvement), a pseudo R-squared was computed based on Cragg & Uhler's approach that falls between 0 and 1:

$$R^2 = \frac{1-\left[\frac{L(null\ model)}{L(model)}\right]^{2/n}}{1-L(null\ model)^{2/n}} \tag{18}$$

where, *n* is the number of observations in the data set. Different models were compared by their R-squared values.

<u>Predictor importance:</u> The absolute value of the z-statistic of each estimated predictor coefficient measures a relative importance of that predictor variable:

$$z_j = \left|\frac{\beta_j}{SE(\beta_j)}\right|,\ j = 1,2,\ldots,k \tag{19}$$

where, *SE* is the standard error.

<u>Cross validation:</u> Predictive performance of the GLMs was measured by cross validation. Observations in each neuron's dataset were split at random into K partitions. GLM fit on K-1 training partitions was repeated and the remaining partition was used for validation. This cross validation was repeated K times at each time one of the partitions served as the validation set.

$$Error = \frac{1}{n}\sum_{k=1}^{K}\sum_{i=1}^{n_k}\left(y_{i,k} - \hat{y}_{i,k}\right)^2\ k \tag{20}$$

<u>Decoding of saccade selection, response choice and orientation change detection:</u> Saccade selection between saccade (hit or FA) and no-saccade (miss or CR) was decoded from spike counts during the test 1 stimulus period based on Bayesian inference of maximum posterior probability using saccade-GLM (**Figure 5D**). According to Bayes' rule, the posterior probability density of the estimated choice given a spike count response is:

$$P(x|Y) = \frac{P(Y|x)P(x)}{P(Y)}\ k \tag{21}$$

where, $P(Y)$ is a normalization term independent of x. Also, assuming that there is no prior knowledge on x, (P (x) = constant), maximizing the posterior is equivalent to maximizing the log-likelihood function used in the GLM encoding model. A random pair of trials one from saccade trial (hit or FA) and another from no-saccade trial (CR or miss) were selected. For each of these two trials, we evaluated the likelihoods of observed spike counts to be consistent with spike counts under the two possible saccade responses for each fitted neuron within a session. Sum of the log-likelihood ratios across neurons amounts the predicted probability of a realization of saccade choice on that trial. If the decoded saccade commitment on both trials of the selected pair match with the observed data, it is only then considered as correct discrimination of a saccade from no-saccade. For choice selection, a pair of trials were randomly selected either hit and miss (nonmatch) or FA and CR (match trial). Prediction accuracy was measured for correct discrimination of hit from miss or FA from CR using saccade-GLM. Similarly, prediction accuracy for orientation change detection was estimated using Δori-GLM. The chance level of prediction is 0.25.

Statistical analysis

Unless otherwise specified, we used paired t-test and multifactor repeated measured ANOVA for comparing normally distributed datasets. Normality was checked with Kruskal-Wallis test.

REFERENCES

Baruni, J.K., Lau, B., and Salzman, C.D. (2015). Reward expectation differentially modulates attentional behavior and activity in visual area V4. Nat Neurosci 18, 1656.

Beatty, J. (1982). Task-evoked pupillary responses, processing load, and the structure of processing resources. Psychol Bull 91, 276.

653 Boudreau, C.E., Williford, T.H., and Maunsell, J.H. (2006). Effects of task difficulty and target
654 likelihood in area V4 of macaque monkeys. J Neurophysiol 96, 2377-2387.

655 Burrows, B.E., Zirnsak, M., Akhlaghpour, H., Wang, M., and Moore, T. (2014). Global selection
656 of saccadic target features by neurons in area V4. J Neurosci 34, 6700-6706.

657 Churchland, M.M., Byron, M.Y., Cunningham, J.P., Sugrue, L.P., Cohen, M.R., Corrado, G.S.,
658 Newsome, W.T., Clark, A.M., Hosseini, P., and Scott, B.B. (2010). Stimulus onset quenches
659 neural variability: a widespread cortical phenomenon. Nat Neurosci 13, 369.

660 Cicmil, N., Cumming, B.G., Parker, A.J., and Krug, K. (2015). Reward modulates the effect of
661 visual cortical microstimulation on perceptual decisions. Elife 4, e07832.

662 Cohen, M.R., and Maunsell, J.H.R. (2009). Attention improves performance primarily by reducing
663 interneuronal correlations. Nat Neurosci 12, 1594-1600.

664 Donahue, C.H., and Lee, D. (2015). Dynamic routing of task-relevant signals for decision making
665 in dorsolateral prefrontal cortex. Nat Neurosci 18, 295-301.

666 Fischer, B., and Boch, R. (1981a). Enhanced activation of neurons in prelunate cortex before
667 visually guided saccades of trained rhesus monkeys. Exp Brain Res 44, 129-137.

668 Fischer, B., and Boch, R. (1981b). Selection of visual targets activates prelunate cortical cells in
669 trained rhesus monkey. Exp Brain Res 41, 431-433.

670 Joshi, S., Li, Y., Kalwani, R.M., and Gold, J.I. (2016). Relationships between pupil diameter and
671 neuronal activity in the locus coeruleus, colliculi, and cingulate cortex. Neuron 89, 221-234.

672 Kimchi, E.Y., and Laubach, M. (2009). Dynamic encoding of action selection by the medial
673 striatum. J Neurosci 29, 3148-3159.

674 Kleinschmidt, A., Büchel, C., Hutton, C., Friston, K.J., and Frackowiak, R.S. (2002). The neural
675 structures expressing perceptual hysteresis in visual letter recognition. Neuron 34, 659-666.

676 Laeng, B., Sirois, S., and Gredebäck, G. (2012). Pupillometry: a window to the preconscious?
677 Perspect Psychol Sci 7, 18-27.

Luo, T.Z., and Maunsell, J.H.R. (2015). Neuronal modulations in visual cortex are associated with only one of multiple components of attention. Neuron 86, 1182-1188.

Maunsell, J.H.R. (2004). Neuronal representations of cognitive state: reward or attention? Trends Cogn Sci 8, 261-265.

McGinty, V.B., Rangel, A., and Newsome, W.T. (2016). Orbitofrontal Cortex Value Signals Depend on Fixation Location during Free Viewing. Neuron 90, 1299-1311.

Moore, T., Tolias, A.S., and Schiller, P.H. (1998). Visual representations during saccadic eye movements. Proc Natl Acad Sci 95, 8981-8984.

Moran, J., and Desimone, R. (1985). Selective attention gates visual processing in the extrastriate cortex. Front Cogn Neurosci 229, 342-345.

Nicolelis, M.A., Dimitrov, D., Carmena, J.M., Crist, R., Lehew, G., Kralik, J.D., and Wise, S.P. (2003). Chronic, multisite, multielectrode recordings in macaque monkeys. Proc Natl Acad Sci 100, 11041-11046.

Padoa-Schioppa, C., and Assad, J.A. (2006). Neurons in the orbitofrontal cortex encode economic value. Nature 441, 223.

Park, I.M., Meister, M.L., Huk, A.C., and Pillow, J.W. (2014). Encoding and decoding in parietal cortex during sensorimotor decision-making. Nat Neurosci 17, 1395.

Pillow, J.W., Shlens, J., Paninski, L., Sher, A., Litke, A.M., Chichilnisky, E., and Simoncelli, E.P. (2008). Spatio-temporal correlations and visual signalling in a complete neuronal population. Nature 454, 995.

Piquado, T., Isaacowitz, D., and Wingfield, A. (2010). Pupillometry as a measure of cognitive effort in younger and older adults. Psychophysiology 47, 560-569.

Reynolds, J.H., and Heeger, D.J. (2009). The normalization model of attention. Neuron 61, 168-185.

Roesch, M.R., and Olson, C.R. (2004). Neuronal activity related to reward value and motivation in primate frontal cortex. Science 304, 307-310.

Rorie, A.E., Gao, J., McClelland, J.L., and Newsome, W.T. (2010). Integration of sensory and reward information during perceptual decision-making in lateral intraparietal cortex (LIP) of the macaque monkey. PloS one 5, e9308.

Saez, R.A., Saez, A., Paton, J.J., Lau, B., and Salzman, C.D. (2017). Distinct roles for the amygdala and orbitofrontal cortex in representing the relative amount of expected reward. Neuron 95, 70-77. e73.

Schiller, P.H., and Lee, K. (1994). The effects of lateral geniculate nucleus, area V4, and middle temporal (MT) lesions on visually guided eye movements. Vis Neurosci 11, 229-241.

Schultz, W., Apicella, P., Scarnati, E., and Ljungberg, T. (1992). Neuronal activity in monkey ventral striatum related to the expectation of reward. J Neurosci 12, 4595-4610.

Shadlen, M.N., and Newsome, W.T. (1998). The variable discharge of cortical neurons: implications for connectivity, computation, and information coding. J Neurosci 18, 3870-3896.

Shiozaki, H.M., Tanabe, S., Doi, T., and Fujita, I. (2012). Neural activity in cortical area V4 underlies fine disparity discrimination. J Neurosci 32, 3830-3841.

Spitzer, H., Desimone, R., and Moran, J. (1988). Increased attention enhances both behavioral and neuronal performance. Science 240, 338-340.

Tremblay, L., Hollerman, J.R., and Schultz, W. (1998). Modifications of reward expectation-related neuronal activity during learning in primate striatum. J Neurophysiol 80, 964-977.

Wang, L., and Ross, J. (1990). Synchronous neural networks of nonlinear threshold elements with hysteresis. Proc Natl Acad Sci 87, 988-992.

Williams, D., Phillips, G., and Sekuler, R. (1986). Hysteresis in the perception of motion direction as evidence for neural cooperativity. Nature 324, 253.

You, H., Meng, Y., Huan, D., and Wang, D.-H. (2011). The neural dynamics for hysteresis in visual perception. Neurocomputing 74, 3502-3508.

Zénon, A., and Krauzlis, R.J. (2012). Attention deficits without cortical neuronal deficits. Nature 489, 434.

ACKNOWLEDGEMENTS

We thank Jackson J. Cone, Zaina Zayyad, Julian Day-Cooney and Thomas Z. Luo for discussion and comments on the manuscript. This work was supported by NIH grant R01EY005911.

AUTHOR CONTRIBUTIONS

S.G. and J.H.R.M. designed the experiments, performed the surgeries and wrote the paper. S.G. performed the experiments and analyzed the data.

DECLARATION OF INTERESTS

The authors declare no competing interests.